Ultrasonic imaging based on frequency-domain optimization form

Samuel Rodriguez, Perrine Sahuguet, Xavier Jacob, Vincent Gibiat

ACOUSTICS 2012

Ultrasonic imaging based on frequency-domain optimization form

S. Rodriguez, P. Sahuguet, X. Jacob and V. Gibiat

Laboratoire PHASE, 118 Route de Narbonne, 31062 Toulouse, France
rodriguez.samuel@yahoo.fr

This paper presents the FTIM (Fast Topological IMaging) method which is based on an optimization method, called the topological sensitivity. The existing methods that use the topological sensitivity have proved to enhance the resolution, but they require extensive computation, as they are based on the numerical simulations of two wave fields. A numerical code such as a time-domain finite-difference scheme is for example used. In the FTIM method, the wave fields are obtained in the frequency domain by multiplying the preliminarily-obtained radiation patterns of the transducers with the Fourier-transformed signals to be emitted. Experimental results obtained with a transducer array are presented for an anisotropic solid, a fluid, and a medium mimicking biological tissues.

1 Introduction

The topological sensitivity methods developed by the mathematical community aim at optimizing a material for given loads and boundary conditions. They have been applied to numerical or experimental electromagnetic and ultrasonic imaging methods [1, 2, 3, 4, 5, 6, 7], such as the TDTE (Time Domain Topological Energy) [1, 2, 3]. The preliminar topological sensitivity analysis for the wave equation shows that an optimal solution of the inverse problem is found by multiplying the solutions of two propagation problems: the direct and the adjoint problems. For both, solid or fluid media, these problems are defined by the propagation of two different sets of waves in the same virtual medium, whose global elastic properties are those of the inspected material. The methods aims at minimizing the cost function defined as the difference between the signals measured and those obtained numerically with the modified medium. The mathematical quantity that represents the location of the inhomogeneities is the gradient of the cost function, the so-called topological gradient, or derivative. Its expression is directly obtained over the whole domain from the solutions $u(\vec{x}, t)$ and $v(\vec{x}, t)$ of respectively the direct and adjoint problems. Its expression depends on the physical problem studied and on the inhomogeneity kind to be detected. However, the integration over the time- (or in the FTIM, frequency-) domain of the product of u and v as in [2] is sufficient to localize all kinds of objects at the first iteration of the optimization process. In the TDTE method, the product of the squared values of the solutions is used to enhance the contrast.

The second section presents the principles of the FTIM (Fast Topological IMaging) method. The direct and adjoint problems are defined and solved in the frequency domain. A new topological derivative is proposed. In the third section, the method is applied to anisotropic media. Experimental results obtained with a composite material sample are presented. In the last section, the method is applied to fluids and experimental results obtained with weakly echogenic inclusions are presented.

2 The Fast Topological IMaging method

2.1 The direct and adjoint problems

First, the experimental data are obtained with a transducer array. Then the direct and adjoint problems are defined as the propagation of two different sets of wave emitted from the virtual array in the virtual medium. Each wave of a set correspond to the excitation signal transmitted to one of the transducers of the virtual array. The set of excitation signals for the direct problem is the set of waves emitted during the experiments. The set of signals for the adjoint problem is the time-reversed (or phase-conjugated in the frequency domain) difference between the signals experimentally measured and the solution of the direct problem restricted to the array location. (Fig. 1)

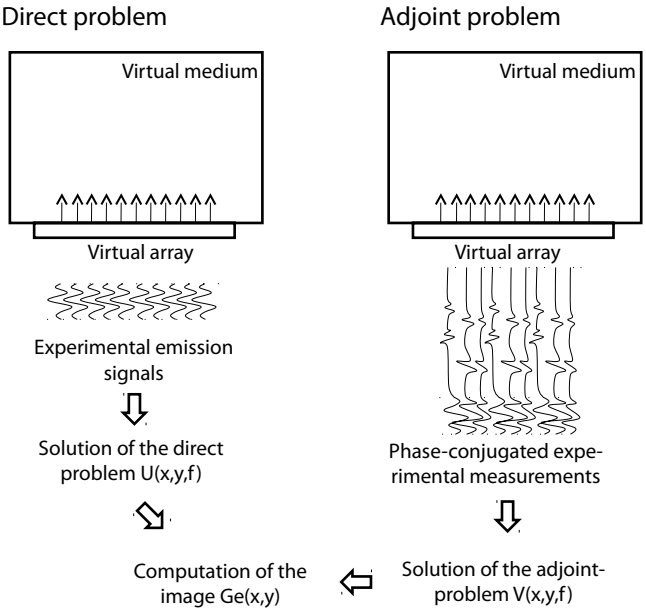

Figure 1: Resolution of direct and adjoint problems. (The signals are plotted in the time domain for clarity)

In this paper, the virtual domains are semi-infinite. The solution of the direct problem restricted to the array is then zero after the duration corresponding to the wave emission. Therefore, the signals emitted in the virtual domain for the resolution of the adjoint problem are the time-reversed measured signals which are set to zero during signal emission. Note that the same virtual domain is used to solve both problems and that only the first iteration of the optimization process is performed as the results obtained are already satisfactory [1].

2.2 The frequency-domain solver

The solutions of the direct and the adjoint problems, respectively $U(\vec{x}, f)$ and $V(\vec{x}, f)$, are obtained as the frequency-domain product of the radiation patterns $H_j(\vec{x}, f)$ of the transducers j and the Fourier-transformed signals to be emitted, following

$$U(x, y, f_k) = \sum_j H_j(x, y, f_k) S_j(f_k) \tag{1}$$

$$V(x, y, f_k) = \sum_j H_j(x, y, f_k) M_j^*(f_k) \tag{2}$$

where H_j is the radiation pattern of transducer j in the virtual domain of Fig. 1; f_k is the kth element of the frequency

vector; S_j is the Fourier-transformed experimental excitation signal transmitted to transducer j; M_j is the Fourier-transformed signal measured by transducer j and preliminarily set to zero during emission. The * symbol corresponds to the complex conjugation. For harmonic traveling waves, it is also called the phase conjugation and can be interpreted as the time-reversal operation.
All the physical information on how the waves propagate in the medium is contained in the radiation patterns H_j. For given medium and array, they are obtained once and for all. It means, that a new image only requires the computations defined in Eq. (1) and Eq. (2). In the experimental applications presented in this paper, all images are 2D and so are U and V.

2.3 The topological derivative definition

With the representation of $\mathcal{G} = \int u(x,y,t)v(x,y,T-t)dt$, where u and v are the time-domain solutions of the direct and adjoint problems respectively and T the simulation duration, the reflective objects can be located precisely [2]. Following extended Parseval's theorem, the gradient is defined in the frequency domain by $\mathcal{G}(x,y) = \int_{\mathbb{R}} U(x,y,f)V(x,y,f)df = 2\Re(\int_{\mathbb{R}^+} U(x,y,f)V(x,y,f)df)$. The topological gradient can be defined on a discrete bounded frequency domain $[f_1 ... f_N]$ as $\Re(G(x,y))$, where $G(x,y)$ is defined by:

$$G(x,y) = \sum_{k=1}^{N} U(x,y,f_k)V(x,y,f_k) \tag{3}$$

In the FTIM method, we represent:

$$G_e(x,y) = |G(x,y)| \tag{4}$$

which equals the norm of $\Re(G) + i\mathcal{H}(\Re(G))$ (where $\mathcal{H}$ is the Hilbert transform), *i.e.* the envelope of the topological gradient $\Re(G)$.

2.4 Comments on the method

The radiation patterns H_j are obtained once and for all for given medium and array. It means that no further numerical simulation has to be performed to obtain a new image from new experimental data. The radiation patterns can be obtained with finite element modeling or from the integration of analytical results, as presented in sections 3 and 4 respectively. In the TDTE method, a finite-difference scheme is used to solve the propagation of the waves in the virtual medium. It means that each new image require a new numerical simulation, which may have a high computation cost.
The use of the frequency domain allow the size of the data to be drastically reduced, as the frequency range of interest is usually small compared to the sampling frequency f_s. For a given frequency range $[f_{min}\ f_{max}]$, the information to store in the frequency domain is $f_s/(2f_{max} - 2f_{min})$ times smaller than in the time domain. In our examples, this ratio equals between 7 and 10.
The use of pre-computed radiation pattern in the frequency-domain dramatically reduces the computation cost. For the experimental results of section 3 for example, the reduction factor is about 60 (from 40 minutes to 40 seconds on the same computer) without compromising the image quality. Furthermore, the simplicity of the numerical operations to be performed make the FTIM method rather easy to embed in a stand alone system.
The radiation pattern of the transducer $j+1$ is easily obtained by translation of that of the transducer j when using a planar transducer array. Thus, all radiation patterns are obtained from only one of them.

3 Application to an anisotropic medium

A 2D finite element model of a semi-infinite composite medium was implemented following [8]. The source is part of the boundary of the domain and is as wide as the transducer of the array, in our case 0.8 mm. The triangular mesh was so designed that there were at least 5 elements per wavelength. The radiation pattern is obtained by interpolating the results of the computation performed for every frequency over a 50 μm regular spatial grid.
The medium experimentally inspected is a composite medium sample presented in Fig. 2. 0.9 mm holes were drilled in the

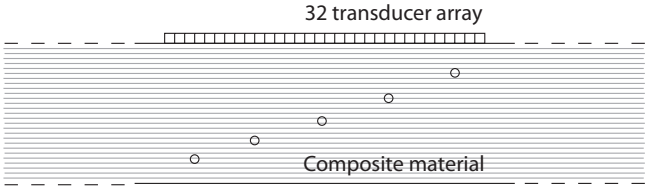

Figure 2: The composite material sample investigated.

sample. The results were obtained with an Imasonic[1] ultrasonic array and a Lecoeur[2] OPEN system. The array was composed of 32 0.8 mm wide transducers in contact with coupling gel. The same experimental excitation signal was applied to all transducers, so that a quasi-plane wave propagated in the medium. The signal was a three-period 5 MHz sinusoidal signal filtered with a Hanning window. The solutions of the direct and adjoint problems are calculated following Eqs. (1, 2) on a 50 μm regular spatial grid. Variable G_e^2 was computed following Eq. (4) and is compared to the result of the TDTE method [2] in Fig. 3. The locations of the objects are the same in both topological images and the images are very alike despite a calculation cost about 60 times lower. The defaults that formed a line, 14 mm deep in the material, correspond to the reflection of the wave at the bottom of the sample, *i.e.* to its thickness. Lateral resolution in TDTE and FTIM is much finer than with a B-scan despite the fact that only one simple plane wave excitation was used. Dominguez *et al.*[1] showed experimentally that a SAFT algorithm was necessary to obtain a resolution similar to that of a one-plane-wave topological image, and the results were nosier.

4 Application to a fluid

In fluids, the radiation patterns were obtained by integrating the analytical green function of a two dimensional semi-infinite medium [9]:

$$-\frac{i}{4}H_0(kr) \tag{5}$$

[1] www.imasonic.fr
[2] www.lecoeur-electronique.com

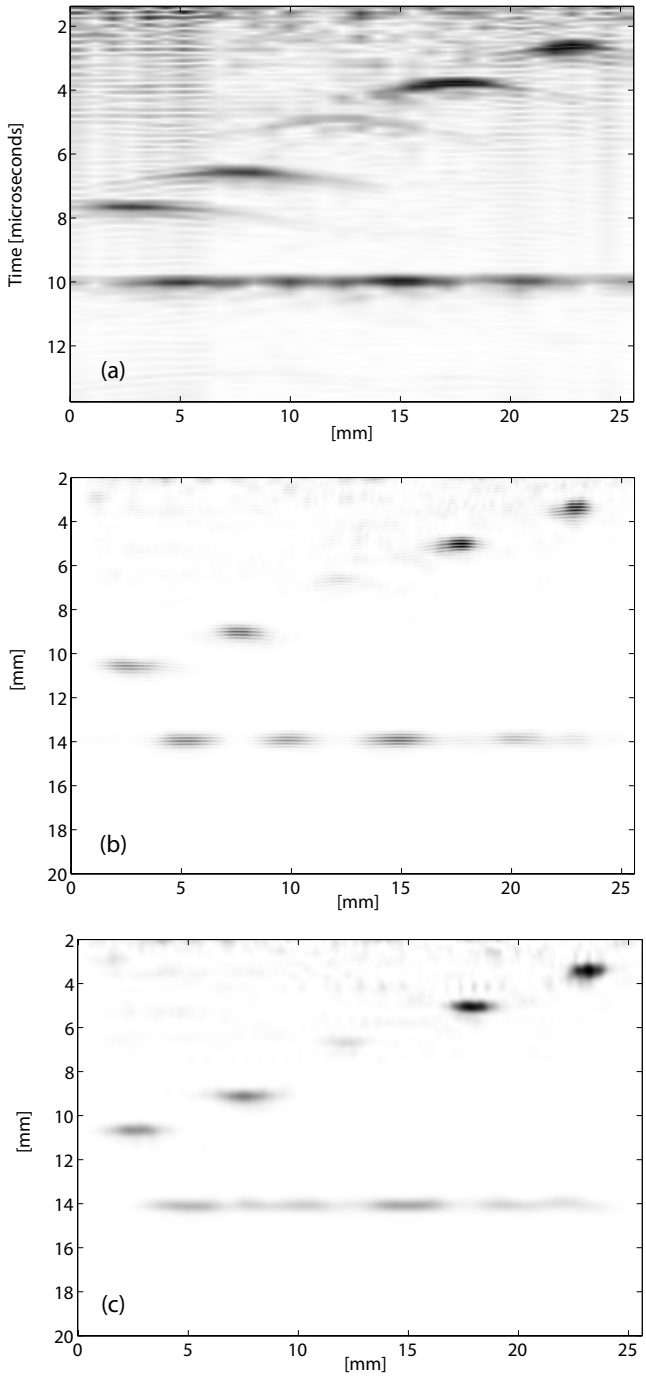

Figure 3: (a) Envelope of the RF signals used as the original experimental data for the calculation of: (b) the TDTE image and (c) the FTIM image squared. The greyscale is normalized over each image.

where H_0 is the zero order cylindrical Hankel's function, r the distance to the source and k the wave number. Assuming an a mm wide planar piston centered in $(x_j, 0)$, the pressure field in the medium is given by:

$$H_j(x, y, f_k) = \int_{x_j - a/2}^{x_j + a/2} -\frac{i}{4} H_0\left(\frac{2\pi f_k}{c} r\right) ds \qquad (6)$$

where $r = \sqrt{(x-s)^2 + y^2}$. The integration is performed with a simple numerical scheme for all (x,y) locations of the grid and for all frequency values of $[f_{min}\ f_{max}]$.
Two experimental configurations were tested. First, a 16 mm gelatin cylinder was immersed in water, so that it appears as a circle in the imaging plane. Second, a hole drilled in a gelatin brick was filled with water. The images obtained with a single plane wave illumination are presented in Fig. 4 and Fig. 5 respectively.
As stated with the composite material, the FTIM greatly improves the lateral resolution of the image. The shape of the gelatin cylinder is precisely defined in Fig. 4 (a). The fact that the shape is obtained is possible because gelatin is a medium similar to water, so that the propagation in those two media are similar. The shape of the water hole in the gelatin medium is also very well defined in Fig. 5 (a). Furthermore a crack in the gelatin is to be seen just under the hole, on its left. The shape of this unwanted, however interesting default appears clearly in the FTIM image, but not on the B-scan. The image in Fig. 5 presents a background noise corresponding to the positions of the small heterogeneities in the gelatin medium. The little bows to be seen around the 20 μs ordinate on Fig. 5 (b) are the signature of two little air bubbles. On the FTIM image of Fig. 5 (a), they appear as two small and precisely defined points, not as large bows.

5 Conclusion

The efficiency of the fast topological imaging method was experimentally checked for elastic waves in solid and fluid media. Lateral resolution for plane-wave excitation is greatly improved, so that the shape of weakly echogenic inclusions can be precisely obtained with the method. The algorithm proposed allows the computation cost to be reduced by about 60 in comparison with existing similar techniques. A real time application of the method is thus made possible.

Acknowledgments

This study was led within the I2MC project funded by the French space and aeronautic foundation STAE (*Sciences et Technologies pour l Aéronautique et l Espace*). The authors would also like to thank Pierre Tella and Pierre de Guibert from the PHASE Laboratory for their essential technical assistance.

References

[1] N. Dominguez, V. Gibiat, "Non-destructive imaging using the time domain topological energy method", *Ultrasonics* **50**, 367-372 (2010).

[2] N. Dominguez, V. Gibiat, Y. Esquerre, "Time domain topological gradient and time reversal analogy: an inverse method for ultrasonic target detection", *Wave Motion* **42**, 31-52 (2004).

[3] P. Sahuguet, A. Chouippe, V. Gibiat, "Biological tissues imaging with time domain topological energy", *Physica Procedia* **3**, 677-683 (2010).

[4] J. Pommier, B. Samet, "The topological asymptotic for the helmholtz equation with dirichlet condition on the boundary of an arbitrarily shaped hole", *SIAM J. Control Optim.* **43**, 899-921 (2004).

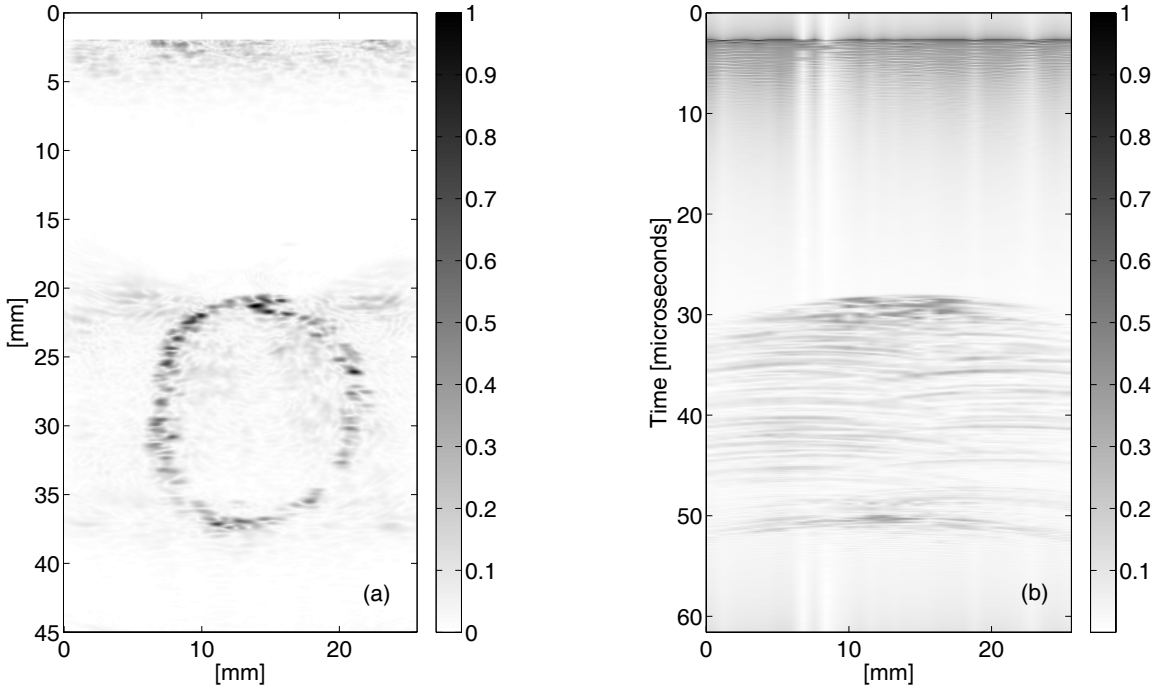

Figure 4: The topological derivative G_e (a) obtained from RF signals whose envelopes are presented in (b). A single plane-wave illumination was applied. The greyscale is normalized over the image.

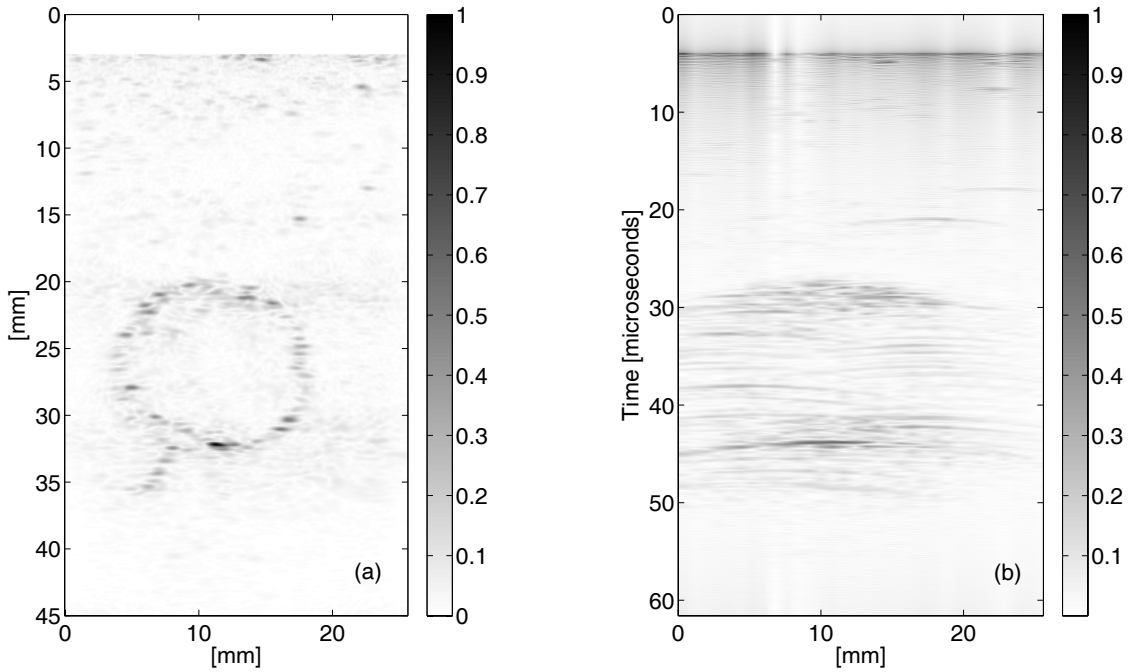

Figure 5: The topological derivative G_e (a) obtained from RF signals whose envelopes are presented in (b). A single plane-wave illumination was applied. The greyscale is normalized over the image.

[5] M. Bonnet, "Topological sensitivity of energy cost functional for wave-based defect identification", *C.R. Mécanique* **338**, 377-389 (2010).

[6] M. Bonnet, "Topological sensitivity for 3d elastodynamic and acoustic inverse scattering in the time domain", *Comput. Methods Appl. Mech. Engrg.* **195**, 5239-5254 (2006).

[7] A. Malcolm, B. Guzina, "On the topological sensitivity of transient acoustic fields", *Wave Motion* **45**, 821-834 (2008).

[8] M. Castaings, C. Bacon, B. Hosten, "Finite element predictions for the dynamic response of thermo-viscoelastic material structures", *J. Acoust. Soc. Am.* **115**, 1125-1133 (2004).

[9] M. Bruneau, T. Scelo, *Fundamentals of acoustics*, ISTE Ltd, 6 Fitzroy Square - London W1T 5DX - UK, 2006, Ch. 3.4.